Applied Catalysis B: Environmental 233 (2018) 202–212

Contents lists available at ScienceDirect

Applied Catalysis B: Environmental

journal homepage: www.elsevier.com/locate/apcatb

Fabrication of BiOI/graphene Hydrogel/FTO photoelectrode with 3D porous architecture for the enhanced photoelectrocatalytic performance

Daimei Chen[a,*,1], Jinjin Yang[b,1], Yi Zhu[b,*], Yuanming Zhang[b], Yongfa Zhu[c,*]

[a] Beijing Key Laboratory of Materials Utilization of Nonmetallic Minerals and Solid Wastes, National Laboratory of Mineral Materials, School of Materials Science and Technology, China University of Geosciences, Beijing 100083, China
[b] Department of Chemistry, Jinan University, Guangzhou, Guangdong, 510632, China
[c] Department of Chemistry, Tsinghua University, Beijing 100084, China

ARTICLE INFO

Keywords:
BiOI
Graphene hydrogel
Electrode
Synergy
Photoelectrocatalysis

ABSTRACT

Three-dimensional (3D) porous networkstructural BiOI-graphene hydrogel-FTO (BiOI/GH/FTO) electrode with remarkably superior photoelectrocatalytic degradation activity and photoelectrocatalytic mineralization ability was successfully prepared by a two-step electrodeposition method. The BiOI nanosheets were electrodeposited into the architectures of 3D porous graphene hydrogel which was prepared by the electrochemical reduction of GO in aqueous dispersion. The morphology and amount of BiOI can be controlled by the electrochemical deposition. With the deposition time of BiOI for 60 s and the working voltage at 1.0 V, the photoelectrocatalytic activity of the 3D BiOI/GH/FTO achieved to the maximum. The removal rate of phenol can be up to about 83% in 5 h, which was 13.8 times higher than that of BiOI/FTO electrode. The degradation rate and mineralization rate of phenol in the solution absence of Na_2SO_4 electrolyte were 76.8% and 56.8%, respectively, which were 13.2 times and 33.4 times as high as that of the BiOI/FTO. The enhanced photoelectrocatalytic degradation activity of 3D BiOI/GH/FTO is due to the 3D porous architecture and a larger surface area of graphene hydrogel which is favorable for reactant diffusion, and the superior electrical conductivity which promotes the charges to transfer excited by BiOI. The BiOI/GH/FTO electrode has the excellent stability. The degradation rates of phenol nearly unchanged after 4 cyclic degradations in static system and a long-term degradation for 72 h in dynamical system. Trapping experiment shows that the hole might be the main active species in photoelectrocatalytic degradation. This research provides new insights in the development of a new photoelectrocatalytic material for the removal of organic compound.

1. Introduction

With the rapid development of social economy and industry, water pollution problems have aroused widespread concern because it is a serious threat to the health of people and the sustainable development of society. There are many methods to removal the water pollutants, such as extraction [1], flocculation precipitate [2], biological oxidation [3], absorption [4], chemical oxidation [5], and photocatalytic or electrochemical catalytic oxidation et al. [6]. Among these methods, photocatalysis as a green advanced oxidation technology exhibits promising potential in wastewater treatment due to its advantages of the use of inexhaustible solar energy, the excellent oxidation ability, low energy consumption and the convenience to large-scale application [7]. However, most of semiconductor photocatalysts have several inevitable shortcomings, including difficulty separation of photocatalyst from suspended water, high electron–hole recombination rate and slow interfacial electron transfer of catalyst which result in the low quantum efficiency.

The combination of semiconductor photocatalysis with electrochemical oxidation (photoelectrocatalytic oxidation) has shown great potential in destruction of organic pollutions in aqueous solution [8]. The applied potential can not only cause the electrochemical degradation of organic pollutions but also promote the photocatalytic activity due to accelerating the charge separation and transfer efficiency. Many photoelectrode materials such as TiO_2 WO_3, $BiVO_4$ and Bi_2MO_6 for PEC cells have been developed for photoelectrocatalytic oxidation [9]. However, none of these materials have reached the performance level required for practical utilization until now. The low separation and transport efficiency of electron-hole is also a key problem to influence the conversion efficiency of photoeletrodes [10].

* Corresponding authors.
E-mail addresses: chendaimei@cugb.edu.cn (D. Chen), tzhury@jnu.edu.cn (Y. Zhu), zhuyf@mail.tsinghua.edu.cn (Y. Zhu).
[1] These two authors contributed equally to this work.

https://doi.org/10.1016/j.apcatb.2018.04.004
Received 14 January 2018; Received in revised form 26 March 2018; Accepted 2 April 2018
Available online 03 April 2018
0926-3373/

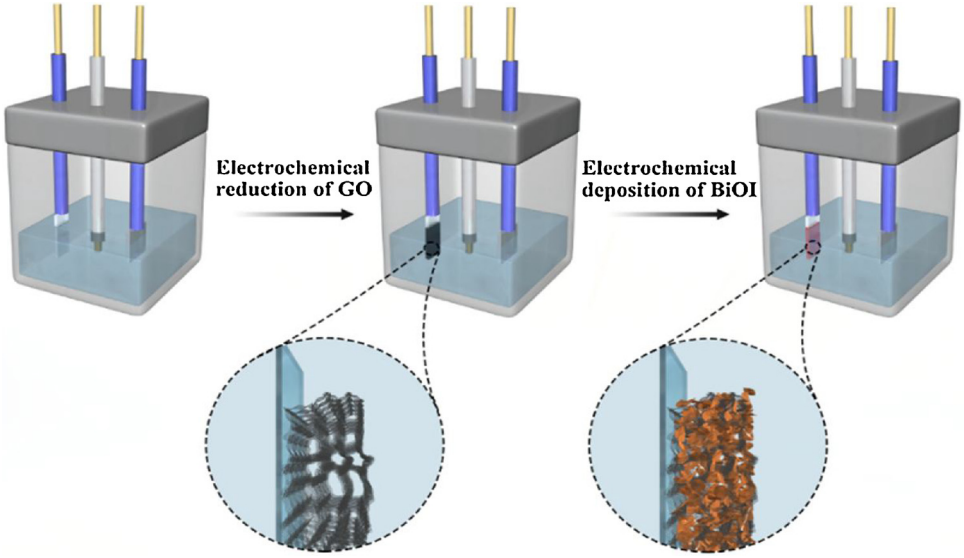

Scheme 1. Schematic illustration of the synthetic process of 3D BiOI/GH/FTO electrode composite by two electrodeposition steps.

Graphene, a two-dimensional material comprised of a monolayer hexagonal sp^2-hybridized carbons, has attracted increasing attention due to its excellent electrical, thermal conductivities, good mechanical properties, and large specific surface area [11]. In particular, the combination graphene with semiconductor are widely regarded as promising electrode materials in PEC application [12] because it can promote the charge carrier transport of semiconductor. Consequently, many graphene based photoelectrod material such as ZnO/graphene, Cu_2O/rGO, $BiVO_4$/rGO and Fe_2O_3/rGO were reported to show the enhanced anodic photocurrents and high PEC conversion efficiency [13]. However, graphene sheets on electrode are easy to self-aggregate forming compact film due to the strong π–π interaction. The aggregation of graphene sheets will dramatically decrease the surface area of the electrode and hinder the electrolyte diffusion inside electrodes. Therefore, graphene based composites with three-dimensional (3D) porous architectures have been developed due to their large surface areas and rapid electrolyte diffusion rate.

Recently, some strategies such as chemical vapor deposition, interferometric lithography have been employed to prepared 3D porous structured graphene and graphene based composite [14]. However, the processes of these methods are complicated and expensive, and high temperature is always required. Polymer adhesion method is most common method to prepare graphene-based catalysts because it is simple and no need the special equipment. Polymer binders act as a linker to connect the graphene with collector. Nevertheless, the poor conductive properties of polymer binders result in the high contact resistance between the graphene based composites and the collector, thus hindering the fast charge transport. Therefore, developing some simply and easily-controllable methods is necessary for electrochemical applications.

Bismuth oxyhalides have been reported as a kind of promising semiconductor photocatalyst with high activity. Among the three bismuth oxyhalides catalysts (BiOX, X = Cl, Br, I), bismuth oxybromide (BiOI) is regarded as a promising visible-light photocatalyst due to a narrow bandgap of 1.8 eV. It is a good photoelectric material and has applied it to photoelectrocatalysis hydrogen production and photodegradation of organic compounds [15–18]. However, the low quantum efficiency limited it for reality application due the high recombination of the photo-generated carries. Thus, it is expected to the combination of BiOI with graphene to accelerate the charge transfer and improve the photoelectrocatalysis efficiency.

The electrochemical deposition has been regarded as an effective and green method to prepare electrode due to that it is facile, fast, and easy-operation. In this work, we aim to develop a kind of new graphene based composite (BiOI/GH/FTO) photo-electrode with 3D porous network structure, and apply it in PEC oxidation in wastewater treatment. BiOI/GH/FTO electrode was prepared by a two-steps electrodeposition method. The reduced graphene sheets were directly deposited on the surface of electrodes by electrochemical reduction of GO, which avoid the harmful reactant and high temperature.The loading amount and morphology of BiOI were controlled by electrochemical deposition to explore the relationship between composition, morphology and PEC efficiency. The BiOI/GH/FTO photo-electrode showed the enhanced photoelectrocatalytic oxidation property for organic compound than pure BiOI/FTO photo-electrode due to the larger surface area, high electrical conductivity and the improved charge carrier separation and transport. The synergistic effect of photocatalysis and electrocatalysis in the organic compounds degradation on BiOI/GH/FTO photo-electrode was discussed in detail. This work provided new insights in rational design of hybrid photoelectrodes for organic pollutant degradation and expanded the photoelectrochemistry in environmental purification.

2. Results and discussion

2.1. Morphology and structure

Scheme 1 illustrated the synthesis of BiOI/GH/FTO electrode by two electrodeposition steps. Firstly, highly porous, conductive 3D graphene hydrogel were prepared by electrochemical reduction of GO on the surface of FTO electrode. Then, BiOI nanosheets were incorporated into the structure of 3D graphene hydrogel by the electrodeposition, forming the 3D BiOI/GH/FTO photo-electrodes. A series of BiOI/GH/FTO photo-electrodes were prepared by controlling the deposition time of BiOI. The microstructure and morphology of as-prepared samples were investigated by the FE-SEM and the HR-TEM. Fig. 1 shows the SEM images of GH, pure BiOI and BiOI/GH composite. As shown that, GH has a 3D porous network structure which was constructed by graphene sheets. The SEM image of BiOI/GH composite showed that BiOI nanosheets grew homogenously into the framework of 3D GH. As the deposition time of BiOI increased, the content of BiOI in BiOI/GH composite increased, more and more BiOI were exposed at the surface of GH, leading to the different morphology of BiOI. When the deposition time of BiOI was less than 60 s, BiOI nanosheets with about 500 nm were homogenously distributed into the framework of 3D porous GH. With the deposition time further increasing, BiOI nanosheets began to self-assemble into the 3D flower-like BiOI microspheres. When the

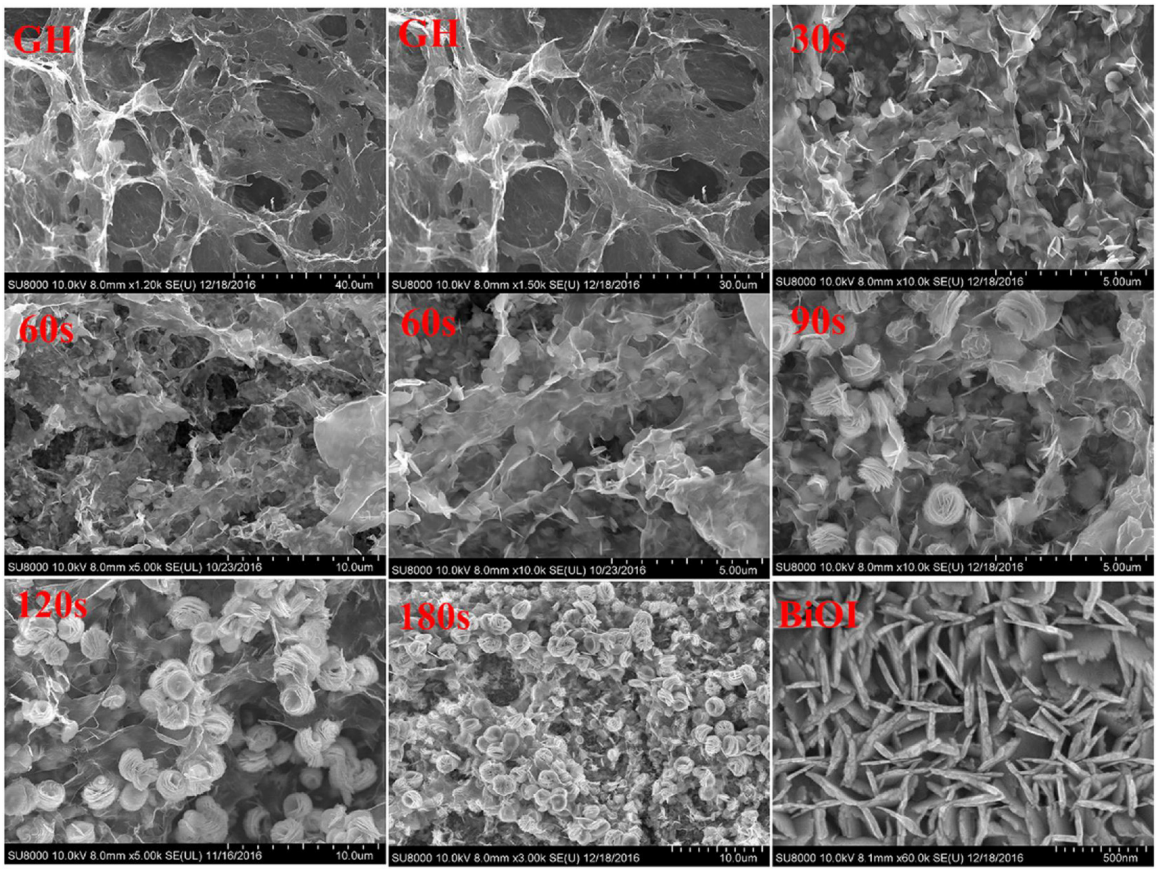

Fig. 1. SEM images of GH, BiOI/GH/FTO electrodes and BiOI/FTO electrode.

deposition time of BiOI was 90 s, both BiOI nanosheets and 3D flower-like BiOI microspheres coexisted in the framework of 3D GH. As the deposition time of BiOI continued to increase, all the BiOI nanosheets in composites have changed into 3D flower-like BiOI microspheres. When the deposition time was up to 180 s, a large number of 3D flower-like BiOI microspheres were aggregated together and overlapped completely on the surface of GH, which might seriously influence the diffusion of electrolyte. The SEM image of BiOI/FTO shows that the uniformed BiOI nanosheets which directly electrodeposited onto the surface of FTO. In a comparison, the BiOI nanosheets in composite are much thinner than that of pure BiOI nanosheets, which might be more favorable for the transfer of photogenerated carriers to the surface of photocatalyst. The SEM images indicated that the presence of graphene and the deposition time of BiOI have some influence on the morphology and structure of BiOI.

The X-ray diffraction (XRD) was used to study the crystal structures of these samples. As shown in Fig. 2, GO has a strong characteristic peak of graphene oxide at $2\theta = 10.8^{\circ}$, and the peak of GO disappeared after the electrochemical reduction process, which indicates that GO has been reduced into the reduced graphene oxide successfully by electrochemical reduction method. The XRD peaks of graphene hydrogels was too weak to be observed in the XRD pattern of BiOI/GH/FTO composites. All the characteristic peaks of BiOI (JCPDS 00-010-0445), corresponding to the tetragonal BiOI, can be observed in BiOI/FTO and BiOI/GH/FTO electrodes, BiOI, suggesting BiOI has deposited on the surface of 3D GH. However, compared with the BiOI/FTO, the peak at $2\theta = 9.7^{\circ}$ dramatically increased and two new distinctive diffraction peaks at $2\theta = 19.4^{\circ}$ and 39.4° appeared in the XRD patterns of BiOI/GH/FTO composite, which can be attributed to the diffraction peak of (001), (002) and (004) crystal planes of BiOI. The fact indicates that the present of graphene hydrogel had a certain influence on growth directions of BiOI, which promotes BiOI crystal to grow along the vertical axis direction. The dominant growth of BiOI in the vertical axis direction may cause some new structural features, which would be confirmed by the HR-TEM.

Raman spectra of as-prepared samples were showed in Fig. 3. As shown that, the Raman bands at 85 cm^{-1} and 147 cm^{-1} of the 3D BiOI/GH/FTO electrode material could belong to the vibration peak of Bi-I bond of the BiOI. The bands at 1348 cm^{-1} and 1585 cm^{-1} can be attributed to the characteristic G band and D band of graphene. The Raman bands of the BiOI/GH/FTO electrode demonstrate that both the BiOI and GH are presented in composite, indicating the successful preparation of BiOI/GH/FTO electrode. Compared to GO, the intensities of G band and D band of graphene in both GH/FTO and BiOI/GH/FTO were significantly enhanced, and the values of I_D/I_G was much higher than that of the GO, indicating that GO was reduced highly by the electrochemical reduction method. The high degree of reduction of GO is favorable to accelerate the transfer of photo-generated electrons of BiOI, thus improving the photoelectrochemical activity of the BiOI/GH/FTO electrodes.

The HR-TEM was used to further study the morphologies and crystal structures of the pure BiOI and BiOI/GH/FTO electrode (shown in Fig. 4). Fig. 4a–c were the HR-TEM images of BiOI/GH/FTO-$_{60s}$ at different magnifications, respectively. The disk-like BiOI nanosheets with the diameter of about 500 nm were homogenously distributed in the 3D network structure of BiOI/GH (Fig. 4a and b). The interplanar distances s of the pure BiOI and the BiOI in BiOI/GH/FTO composite are about 0.267 nm and 0.282 nm, corresponding to the (111) and (110) facets of BiOI, respectively. Both the pure BiOI and the BiOI of BiOI/GH/FTO composite mainly exposed the (111) and (110) facets (Fig. 4c and d). And a much thinner BiOI nanosheet can be observed much more clearly through HR-SEM image. The HR-TEM images confirmed that the dominant growth of BiOI in vertical axis direction did not affect the exposure of the crystal plane of BiOI. Fig. 5 shows the

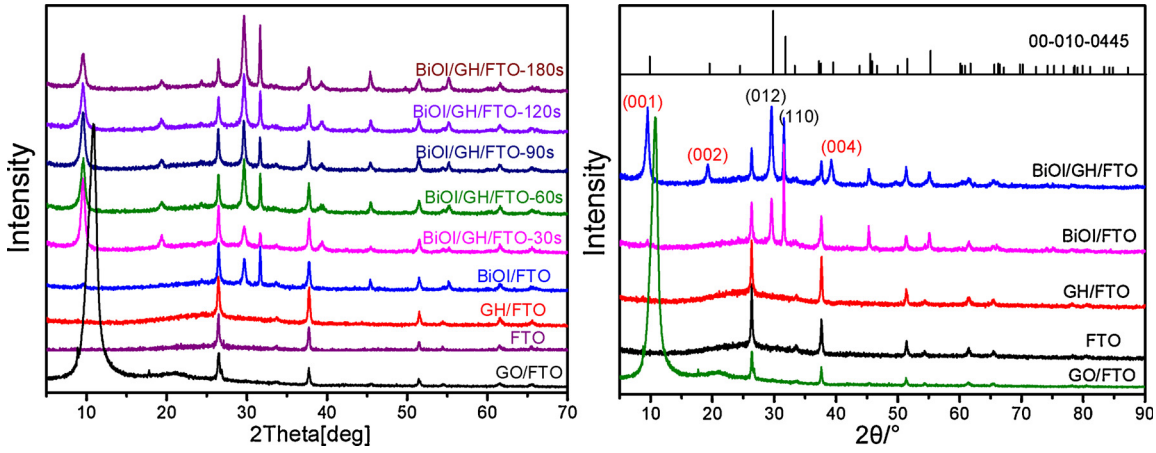

Fig. 2. The XRD patterns of GO, GH/FTO, BiOI/FTO and BiOI/GH/FTO composites.

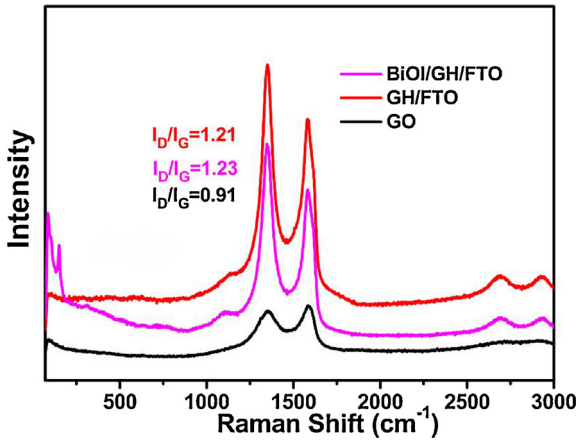

Fig. 3. Raman spectra of GO, GH/FTO and BiOI/GH/FTO.

EDX of BiOI/GH-$_{60s}$ composite and its corresponding EDX mappings, which demonstrates that there are only Bi, O, I and C elements existing in the BiOI/GH-$_{60s}$ composite and BiOI are evenly distributed.

Fig. 6 shows the UV–vis diffuse reflectance spectra (DRS) of BiOI/FTO, GH/FTO and BiOI/GH/FTO electrodes. As Fig. 6 presented, the BiOI/FTO has a high visible light absorption with the optical absorption band edge at about 635 nm. The optical absorption edge of BiOI/GH/FTO electrode exhibited an apparent red shift gradually with the increase of graphene hydrogel, suggesting that the graphene hydrogel can improve the light absorption of BiOI/GH/FTO sample. The light absorption intensity of the BiOI/GH/FTO in both UV and visible light regions decreased gradually with the decrease of BiOI, and all of them are much lower than that of the BiOI/FTO electrode. The reason can be attributed to the 3D porous structure of the BiOI/GH/FTO electrode, through which the light can pass the void and the reflected photons decreased, resulting in the light absorption intensity of BiOI/GH/FTO electrode decreased. The special 3D framework of BiOI/GH/FTO electrode is beneficial to the spread of light inside the composite, which could improve the light harvest and enhance the photocatalytic activity. GH/FTO electrode, as a black material, exhibits a very strong absorption in the whole UV and visible light regions.

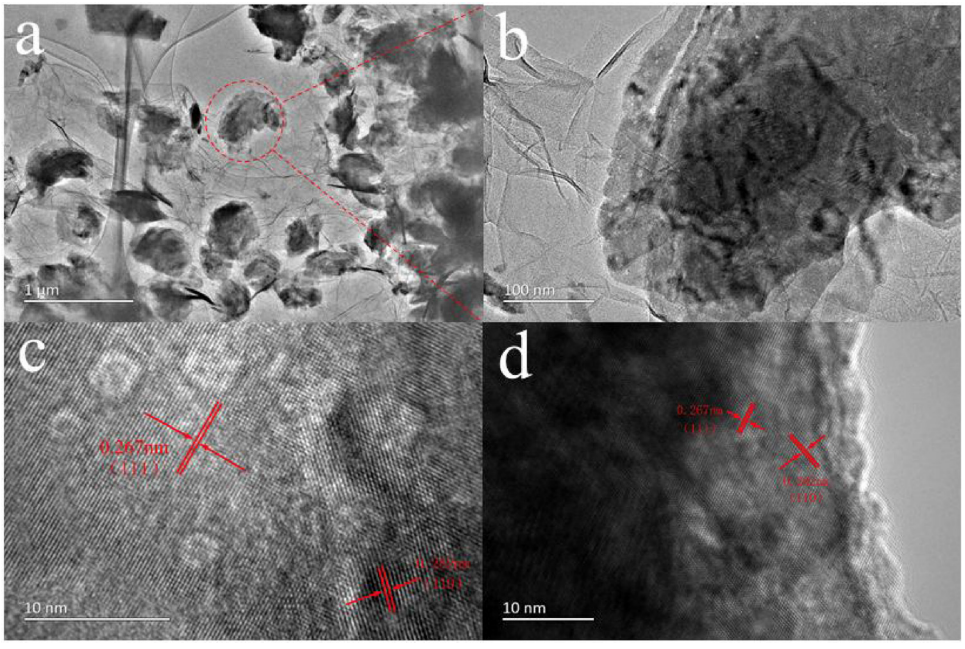

Fig. 4. The HR-TEM images of (a–c) BiOI/GH-$_{60s}$ and (d) the pure BiOI.

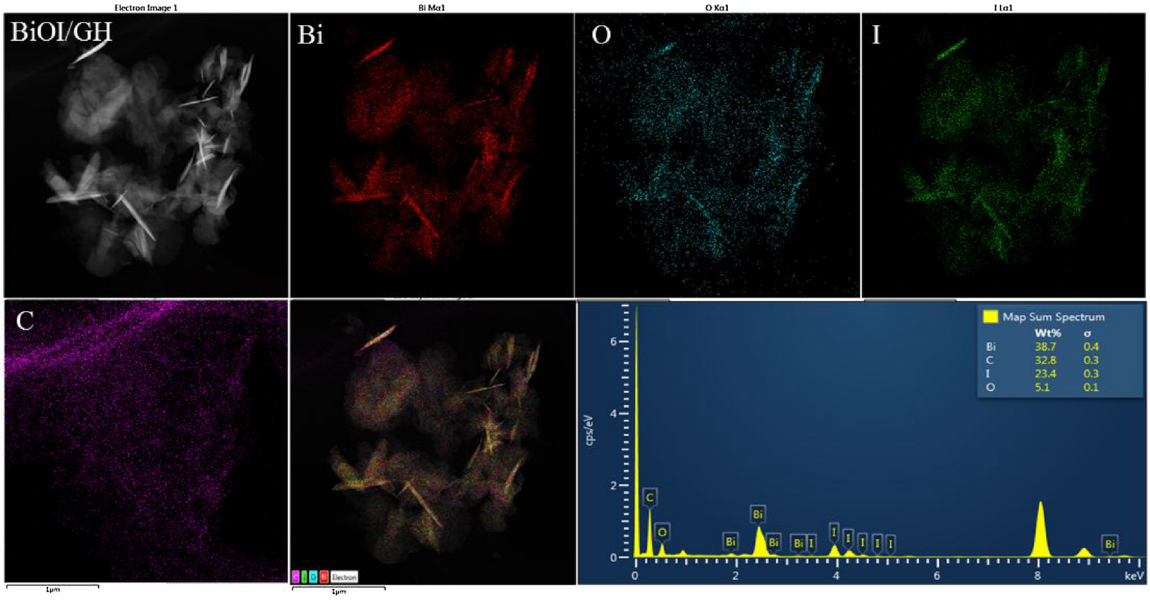

Fig. 5. The EDX of BiOI/GH/FTO-$_{60s}$ and its corresponding EDX mappings of C, Bi, O and I elements.

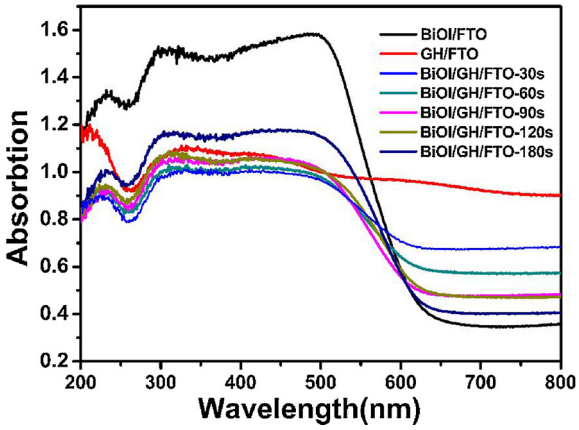

Fig. 6. The UV–vis diffuse reflectance spectra (DRS) of GH/FTO, BiOI/FTO and BiOI/GH/FTO electrodes.

2.2. The PEC degradation of phenol in static system

The PEC degradations over different electrodes under visible light (λ ≥ 420 nm) in static system are showed in Fig. 7. 5 ppm of phenol solution contains 0.1 M Na_2SO_4 was used as target pollution compound. As shown in Fig. 7a, phenol hardly has any self-degradation under the visible light, indicating that phenol has a very high photostability. All the BiOI/GH/FTO photo-electrodes have high PEC degradation efficiency for phenol at a constant applied voltage (E = 1.0 eV), and the degradation rate of phenol firstly increased and then decreased with the increase of the deposition time of BiOI. Fig. 7b shows the corresponding reaction rate constant of phenol degradation over BiOI/GH/FTO photo-electrodes. The reaction rate of photoelectrocatalytic degradation of phenol increased gradually before the deposition time of BiOI 60 s, after that the degradation rate decreases. When the deposition time of BiOI is 60 s, the BiOI/GH/FTO electrode has the maximum reaction rate constant ($k = 0.35\ h^{-1}$), suggesting that the excessive BiOI worsens the PEC degradation activity.

In order to confirm the synergistic effect of photocatalytic degradation and electrocatalytic degradation of the BiOI/GH/FTO electrode, the comparison of photocatalytic degradation, electrocatalytic degradation and the photoelectrocatalytic degradation of phenol over BiOI/GH/FTO$_{-60s}$ photo-electrode were conducted in static system. As shown in Fig. 8a, the BiOI/GH/FTO$_{-60s}$ electrode can hardly decompose phenol just under the visible light. However, it has good electrocatalytic activity for phenol degradation with removal rate was about 65% in 5 h. In a contrast, the PEC degradation rate of phenol over the BiOI/

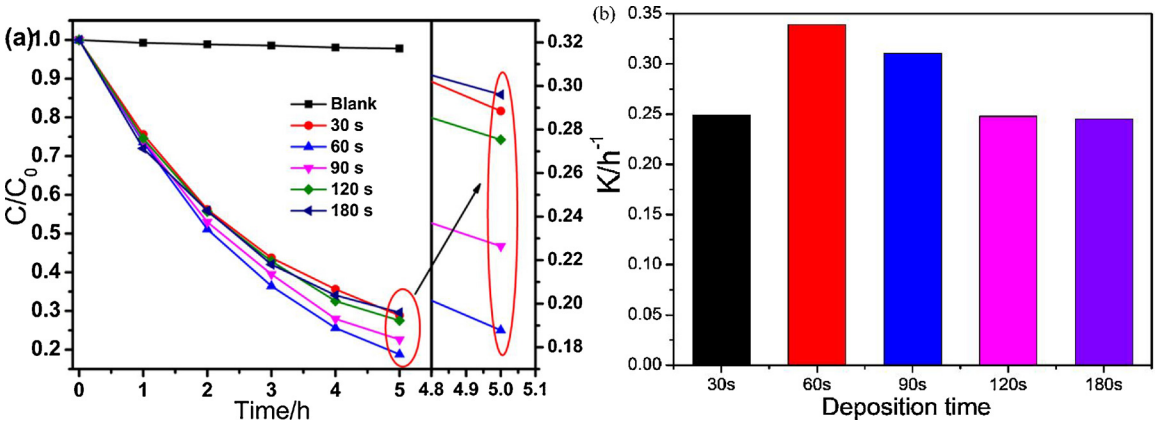

Fig. 7. (a) The PEC degradation over different BiOI/GH/FTO photo-electrodes under visible light (λ ≥ 420 nm) in static system, and (b) the corresponding reaction rate constant.

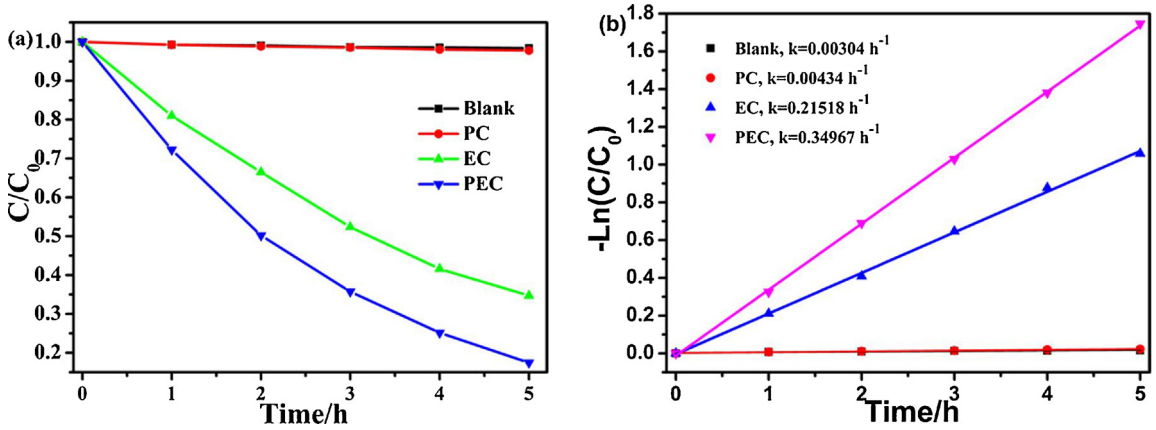

Fig. 8. (a) The photocatalytic, electrocatalytic and the PEC degradations of phenol over the BiOI/GH/FTO$_{-60s}$ electrode under visible light (λ ≥ 420 nm) in static system, and (b) its corresponding kinetic simulation curves.

GH/FTO$_{-60s}$ electrode can reach nearly 83% in 5 h which was much higher than those of the electrocatalytic degradation and photocatalytic degradations of phenol. The result confirms that the synergistic effect of photocatalysis and electrocatalysis of the BiOI/GH/FTO photo-electrode can greatly improve the degradation rate of phenol. The kinetic study exhibits that the synergistic degradation of phenol over BiOI/GH/FTO belongs to the quasi-first-order kinetics (Fig. 8b). The PEC degradation rate constant (k) of BiOI/GH/FTO$_{-60s}$ is 0.35 h^{-1}, which is about 1.63 and 81.4 times higher than that of the electrocatalytic degradation and photocatalytic degradation, respectively.

Fig. 9 gives the comparison of the PEC degradations of phenol over BiOI/GH/FTO$_{-60s}$ and BiOI/FTO$_{-60s}$ photo-electrodes. As shown in Fig. 9a, the PEC degradation rate of phenol over BiOI/GH/FTO photo-electrode was nearly 83% in 5 h, which was 13.8 times higher than that of BiOI/FTO$_{-60s}$ photo-electrode. The reaction rate constant (k) of phenol degradation over the BiOI/GH/FTO$_{-60s}$ photo-electrode was about 17 times higher than that of the BiOI/FTO$_{-60s}$ photo-electrode. The experimental result indicates that the presence of graphene hydrogel greatly enhances the photoelectrocatalytic activity of the BiOI/GH/FTO photo-electrode This might be that the 3D porous graphene hydrogel not only is favorable for the diffuse of reactants and increase the contact chances between the reactants and catalysts, but also can promote the separation and transfer of electron-hole pairs.

The applied voltage is one of the most important factors that affect the PEC degradation efficiency of the BiOI/GH/FTO photo-electrode. To investigate the influence of applied voltage on the PEC degradationefficiency the BiOI/GH/FTO$_{-60s}$ photo-electrode, the experimental test was conducted in static system at different work voltages. Fig. 10a and b showed the degradation curves and corresponding reaction rate constant (k) of phenol over the BiOI/GH/FTO$_{-60s}$ photo-electrode with the different applied voltage ranging from 0.8 V–1.3 V. As shown that, the degradation rate of phenol firstly increased and then decreased with the increase of the applied voltage, and when the applied voltage was 1.0 V, the BiOI/GH/FTO$_{-60s}$ photo-electrode had the highest degradation rate of phenol.

Fig. 11 shows the PEC degradation over the BiOI/GH/FTO$_{-60s}$ photo-electrode in the solution with or without Na_2SO_4 as electrolyte. As shown that, phenol can also hardly photocatalytic degrade in the solution absence of Na_2SO_4 under visible light. However, the BiOI/GH/FTO$_{-60s}$ photo-electrode still has high electrocatalytic activity and photoelectrocatalytic activity for phenol degradation in the solution without Na_2SO_4 electrolyte, and the degradation rate just has a slight decline compared to that in the solution containing Na_2SO_4. In details, the electrocatalytic degradation rate and the PEC degradation rate of phenol were decreased by about 9% and 5%, respectively. The result shows that the electrolyte in the phenol solution has certain influences on both the electrocatalytic activity and the PEC activity of the BiOI/GH/FTO photo-electrode. The slight decline of phenol degradation rate demonstrated that the electrolyte just has a little effect on the PEC degradation on the BiOI/GH/FTO photo-electrode, which is beneficial to enlarge the application of the BiOI/GH/FTO photo-electrode.

Fig. 12 shows the degradation rates of phenol over the BiOI/GH/FTO$_{-60s}$ and BiOI/FTO$_{-60s}$ photo-electrodes under different experimental conditions, and their corresponding mineralization rates of phenol in the solution without Na_2SO_4 electrolyte. According to Fig. 12, the degradation rates of phenol by photocatalytic degradation,

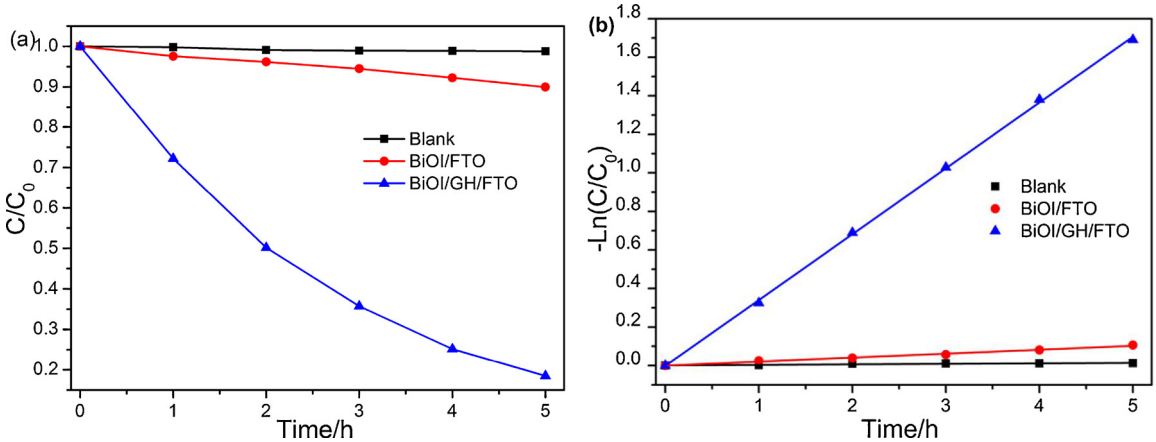

Fig. 9. (a) The comparison of the PEC dedradations of phenol over BiOI/GH/FTO$_{-60s}$ and BiOI/FTO$_{-60s}$ electrodes, and (b) the corresponding kinetic simulation curves.

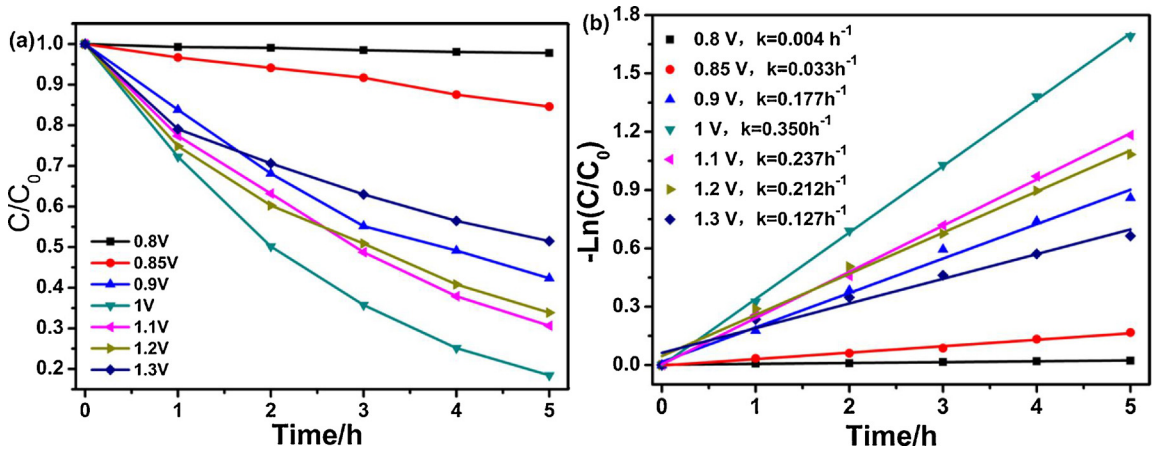

Fig. 10. (a) The PEC degradations of phenol on the BiOI/GH/FTO$_{-60s}$ photo-electrode at different applied voltages, (b) the corresponding kinetic simulation curves and reaction rate constants.

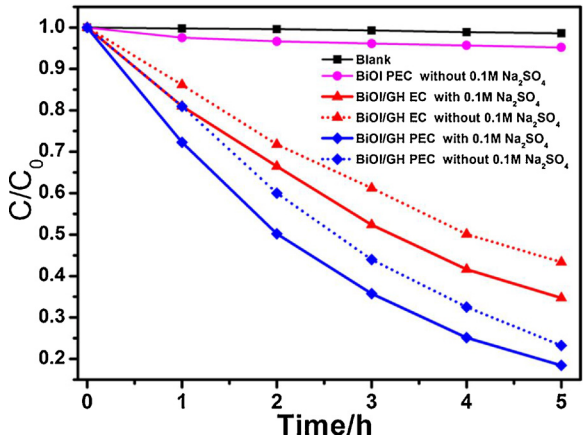

Fig. 11. The PEC degradation of phenol with or without Na_2SO_4 as electrolyte over the BiOI/GH/FTO$_{-60s}$ photo-electrode.

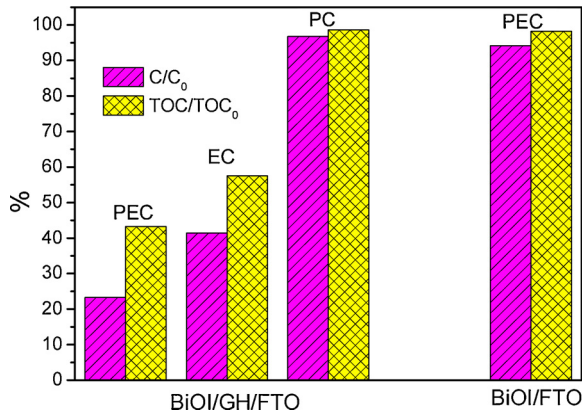

Fig. 12. Degradation rates and mineralization rates of phenol over the BiOI/GH/FTO$_{-60s}$ and BiOI/FTO$_{-60s}$ photo-electrodess in the solution without Na_2SO_4.

electrocatalytic degradation and the PEC degradation over the BiOI/GH/FTO$_{-60s}$ photo-electrode were 3.2%, 58.6% and 76.8%, respectively, and their corresponding mineralization rates were 1.4%, 42.5% and 56.8%, respectively. The PEC degradation over BiOI/GH/FTO$_{-60s}$ photo-electrode has the high mineralization ability and 56.8% of phenol can be completely mineralized into carbon dioxide and water. In a contrast, the degradation rate and the mineralization rate of phenol by the PEC degradation over the BiOI/FTO$_{-60s}$ photo-electrode were much lower than those of the BiOI/GH/FTO$_{-60s}$ photo-electrode, the PEC degradation rate and mineralization rate were 5.8% and 1.7% respectively. The result indicates that the existence of 3D porous graphene hydrogel can highly enhance the PEC degradation of the BiOI/GH/FTO$_{-60s}$ photo-electrode. The reason might be that the excellent electrical property of graphene can accelerate the separation and transfer of electron-holes pairs from BiOI, and 3D porous structure is helpful for the diffuse of the reactant in solution.

The high performance liquid chromatography (HPLC) can be used to record the intermediate products of phenol solution during the PEC degradation over the BiOI/GH/FTO photo-electrode. As shown in Fig. 13, the peak intensity of phenol at t = 3.52 min gradually reduced during the reaction process. While the peak intensities of intermediate products at t = 1.91 min and t = 2.46–2.6 min have a little increase with prolonging irradiation time. According to the report of the literature [19], the intermediate products of phenol can be attributed to hydroquinol and p-benzoquinone/catechol. In addition, the peak intensities of the intermediate products increased much slower compared to the decrease of the peak of phenol with prolonging degradation time, which indicated that most of the intermediate products of phenol were completely mineralized into carbon dioxide and water during the PEC degradation process.

2.3. Mechanism

The synergistic effect of photoelectrocatalytic degradation of the BiOI/GH/FTO electrode can be further explored by transient photocurrent response. As shown in Fig. 14, the transient photocurrents of

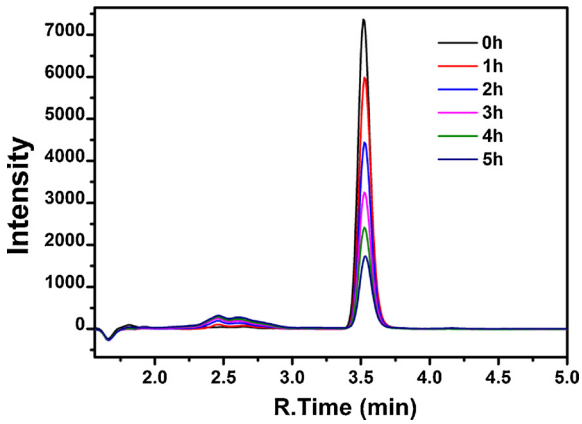

Fig. 13. HPLC chromatograms of PEC degradation of phenol over the BiOI/GH/FTO$_{-60s}$ photo-electrode under visible light irradiation.

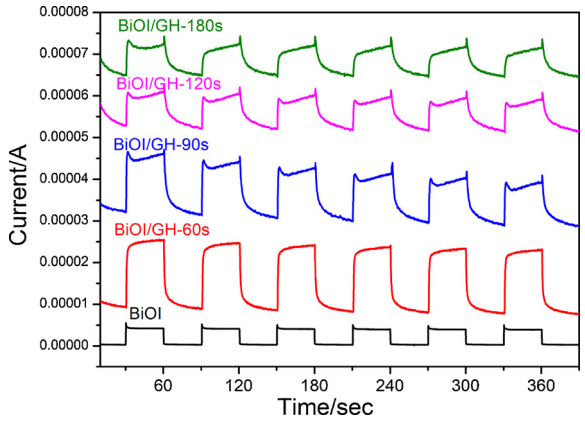

Fig. 14. Transient photocurrent responses of BiOI/GH/FTO and BiOI/FTO electrodes.

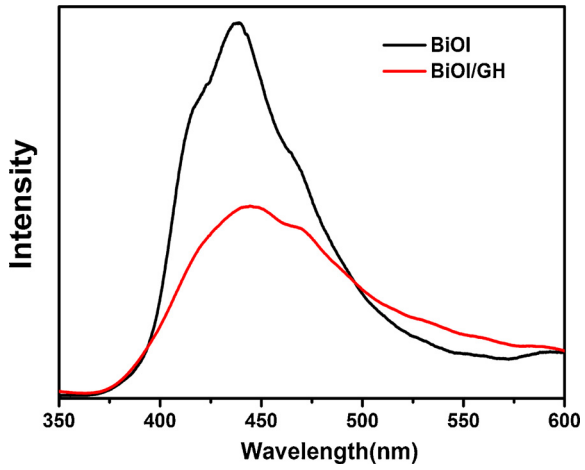

Fig. 15. PL spectra of the pure BiOI and BiOI/GH composite.

the all 3D BiOI/GH/FTO electrodes are much higher than that of the pure BiOI. The BiOI/GH/FTO$_{-60s}$ electrode has the highest photocurrent response (2.54×10^{-5} A), which is 5.9 times that of the pure BiOI (4.27×10^{-6} A). The change trend of photocurrent of the BiOI/GH/FTO is consistent with the PEC degradation efficiency. The enhanced photocurrent response can be attributed to the excellent conductivity of graphene, which is conducive to the rapid transfer of photogenerated electrons; on the other hand, the 3D porous structure of the composite hydrogel can prevent the aggregation of BiOI, and the 3D graphene hydrogel can provide multi-dimensional transfer paths for photo-generated electron, which could accelerate the transfer of photo-generated electrons and enhances the photocurrent response. Fig. 15 shows the photoluminescence spectra (PL) of the composite hydrogel and the pure BiOI. In a comparison, the PL peak intensity of the BiOI/GH/FTO composite is much lower than that of the pure BiOI, which indicates that GH hindered the recombination of the photo-generated electron and hole. Based on above results, it can be concluded that the 3D BiOI/GH/FTO composite hydrogel accelerated the separation and transfer of photo-generated carriers and hindered their recombination, thus improves the photocatalytic activity of BiOI/GH/FTO.

Main oxidative species during the photoelectric degradation process over phenol using the BiOI/GH/FTO electrode were detected by the trapping experiments of radicals using isopropanol (IPA) as hydroxyl radical scavenger [20], formic acid (FA) as holes radical scavenger [21] and benzoquinone (BQ) as superoxide radical species ($\cdot O^{2-}$) scavenger [22]. Fig. 16 shows that the PEC degradation of phenol over BiOI/GH/FTO$_{-60s}$ hardly has any change by the addition of IPA in the reaction system, and BQ just has a slight influence on photoelectrocatalytic

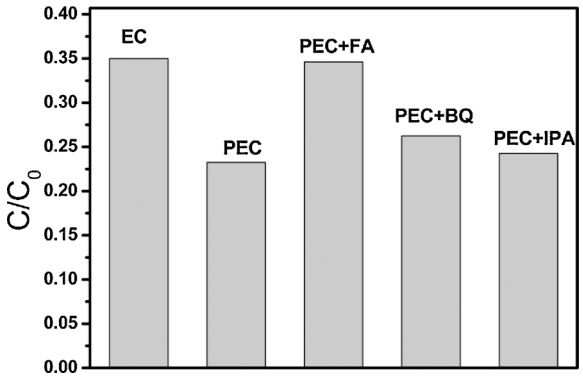

Fig. 16. The trapping experiments of active species over GH/BiOI/FTO$_{-60s}$.

degradation, while the degradation rate of phenol over the BiOI/GH/FTO$_{-60s}$ photo-electrode was significantly decreased with the addition of formic acid, indicating that the holes (h^+) acts as one type of the main oxidative species for BiOI/GH/FTO composite. The trapping experiments imply that phenol is main oxidized directly by holes rather than that ·OH. Most of the photogenerated electrons are transferred to the cathode through the external circuit, just a small amount of photogenerated electrons react with the dissolved oxygen in the solution to produce superoxide radicals.

According to the above analysis, BiOI/GH/FTO electrode remarkably improved the photoelectrocatalytic oxidation performance under visible light irradiation. The possible mechanisms of PC, EC and PEC degradation processes were as follows: in the degradation processes of BiOI/GH/FTO photoelectrode, 3D GH can absorb and enrich phenol molecular rapidly onto the surface of the BiOI nanosheets due to the 3D porous structure and the strong π-π interaction. Furthermore, graphene, as a good electronic conductor, can improve the charge separation and transfer efficiency of BiOI/GH/FTO electrode, and the 3D network of GH can provide multidimensional quality and electron transfer channels, which is in favor of the rapid transmission of pollutant molecules and electrons, thus greatly enhance the photocatalytic performance. In the photocatalytic process, BiOI of BiOI/GH/FTO electrode was excited and generated photo-generated electrons (e^-) and holes (h^+), and e^- on the conduction band (CB) of BiOI can transfer to GH, thus improved the effective separation of photo-generated electrons and holes, and exhibited the photocatalytic degradation activity. In the electrocatalytic process, GH of BiOI/GH/FTO composite has much better electrochemical property and electrical conductivity compared to BiOI. When applied voltage on the composite electrode, it mainly reflects the electrocatalytic activity of graphene. The additional anode voltage is equivalent to the injection of holes on the anode material to degrade the organic pollutants. In the photoelectrocatalytic degradation process (shown in Fig. 17), the BiOI of BiOI/GH/FTO electrode was excited and generated photo-generated electrons (e^-) and holes (h^+) under the visible light, and the electrons transferred to GH rapidly and then transported to the counter electrode through an external circuit. Meanwhile, the applied voltage prompted the photo-generated electrons to move to the external circuit rapidly, which greatly reduced the recombination of photogenerated electron and hole. The holes left on the valence band of BiOI have strong oxidation ability, which can completely degrade the organic pollutant molecules that adsorbed on the surface of catalyst into CO_2 and H_2O. Therefore, the 3D porous structure and the excellent electronic property of 3D graphene hydrogel have the synergistic effect of PEC degradation of phenol over BiOI/GH/FTO electrode, thus highly increase removal efficiency of organic compound.

2.4. Stability of the 3D composite hydrogel photo-electrode

To investigate the stability of PEC degradation over the BiOI/GH/

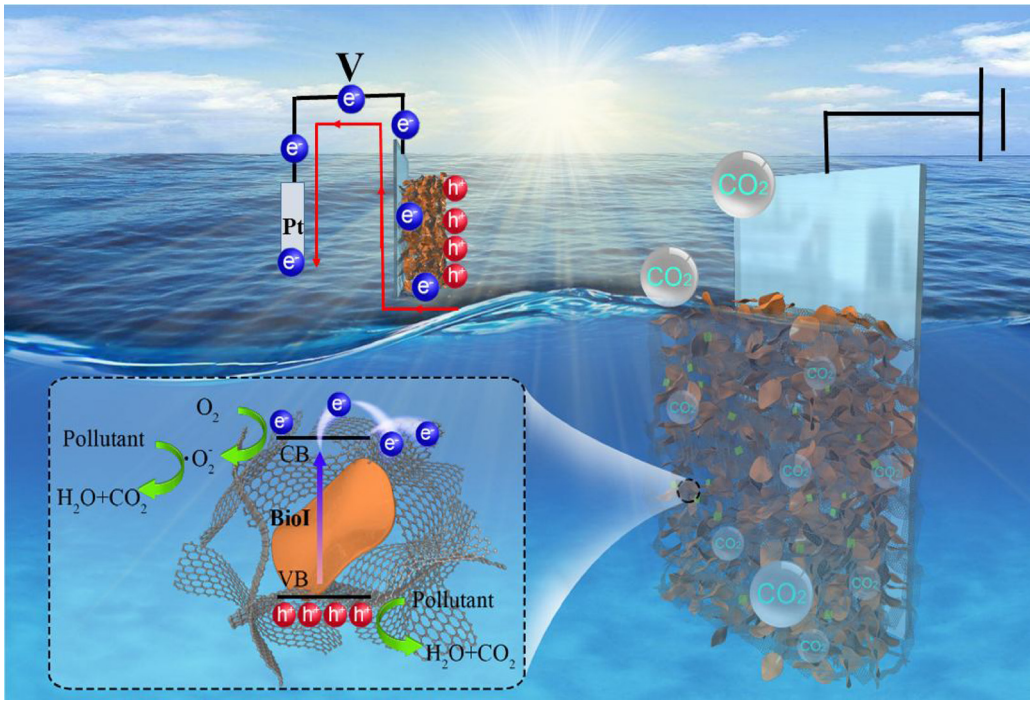

Fig. 17. Schematic drawing illustrates the PEC degradation by BiOI/GH/FTO photo-electrode.

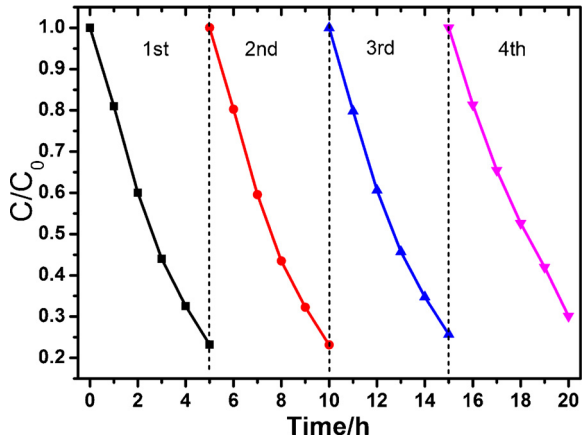

Fig. 18. The circulation experiments of phenol degradation over the BiOI/GH/FTO$_{-60s}$ photo-electrode in the solution absence of Na_2SO.

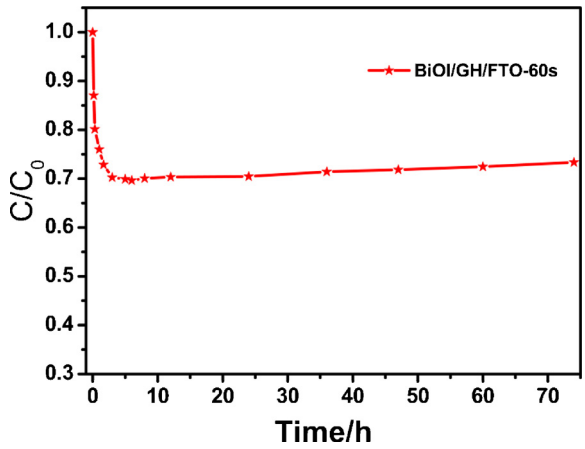

Fig. 19. The PEC degradation over the BiOI/GH/FTO$_{-60s}$ photo-electrode in dynamic system.

FTO$_{-60s}$ photo-electrode, the circulation experiment conducted in static system and a long-term detection of phenol solution in dynamic system were carried out. The flow rate of phenol solution was 1.2 mL/min in dynamic system. As shown in Fig. 18, the BiOI/GH/FTO$_{-60s}$ photo-electrode exhibited an excellent cycling stability for phenol removal. The photoelectrocatalytic degradation rate of phenol remained unchanged after the fourth cycle degradation. Fig. 19 showed the result of the stability property of PEC degradation of phenol over the BiOI/GH/FTO$_{-60s}$ photo-electrode in dynamic system. The concentration of the effluent phenol solution decreases quickly with continuous fresh phenol solution flowing through the BiOI/GH/FTO$_{-60s}$ photo-electrode in the initial 3 h and then kept nearly unchanged for the last 74 h degradation. In details, the degradation rate of phenol reached up to 31% after 3 h, and it just has a slight decrease for the last 74 h with the degradation rate of about 26% in dynamic system, which can be attributed to the excellent synergistic effect of photoelectrocatalytic degradation of the BiOI/GH/FTO$_{-60s}$ photo-electrode and its high stability. The results indicate that the 3D porous BiOI/GH/FTO photo-electrode has the high PEC degradation efficiency and excellent stability property in dynamic system, whichmight be a suitable material to be utilizedin pollutants treatment in reality.

3. Conclusions

In this work, BiOI/GH/FTO composite photo-electrode with 3D porous network structure was successfully prepared the electrodeposition method. This method for the preparation of graphene hydrogel composite electrode is simple, rapid and easy to operate. The 3D composite graphene hydrogel photo-electrode achieves much higher PEC degradation efficiency and mineralization rate for organic pollutant than the BiOI/FTO composite photo-electrode due to the 3D porous structure of graphene hydrogel, which is favorable for diffusion and absorption of electrolyte, and the excellent electronic property, which can promote the separation and transfer of electron-hole pairs. The 3D BiOI/GH/FTO photo-electrode has the high stability in both circulation experiments and dynamic system, showing the potential application in industry This research provides new ideas and insights into the fabrication of hydrogel-based composite photo-electrode for scale and

expands the potential application for the PEC oxidation technology in the field of water purification.

4. Experimental

4.1. Preparation of 3D-BiOI/GH/FTO electrode materials

4.1.1. Preparation of 3D-GH/FTO electrode

All chemicals were of analytical grade and used without further purification. Graphene oxide (GO) solution was prepared by the ultrasonic treatment of graphene oxide mud and water for 30 min. The 3D graphene hydrogel electrodes can be prepared by electrochemical reduction method [15,23], employing a three-electrode system consisting F-doped SnO_2 coated glass (FTO) (area of $2 \times 4\ cm^2$) as working electrode, Pt wire as counter electrode and SCE as reference electrode. Before the electrochemical reduction of GO, the FTO should be modified with 3-Amino-propyltriethoxysilane (APTES) to ensure the as-deposited 3D graphene hydrogel stick on FTO firmly. The FTO glasses was firstly immersed into a 0.5% (v/v) APTES ethanol solution for 1 h, and then washed it thoroughly with ethanol, dried it for 2 h at the temperature of 120 °C. The electrodeposited 3D-GH/FTO electrode was conducted at a constant potential of −1.25 V for 150 s. The electrolyte was a suspension of 4 mg/mL graphene oxide solution containing 0.12 M $LiClO_4$. Finally, the as-prepared 3D-GH/FTO electrode was then immersed in DI water to remove excessive GO and $LiClO_4$.

4.1.2. Preparation of 3D-BiOI/GH/FTO electrode

The 3D-BiOI/GH/FTO electrode was prepared by the electrodeposition of BiOI on the surface of 3D-GH in a three-electrode cell which was constructed with the as-prepared 3D-GH/FTO working as the working electrode, a Pt wire served as the counter electrode and SCE as the reference electrode. Electrolyte solution was prepared as follows: 50 mL of solution containing 0.04 M $Bi(NO_3)_3$ and 0.4 M KI with pH adjusted to 1.7 by adding HNO_3 was mixed with 20 mL of the absolute ethanol (100%) containing 0.23 M p-benzoquinone. A series of 3D-BiOI/GH/FTO electrodes with different deposition time were prepared by cathodic deposition which was performed potential statically at −0.15 V vs. SCE at room temperature, denoting as BiOI/GH/FTO$_{-30s}$, BiOI/GH/FTO$_{-60s}$, BiOI/GH/FTO$_{-90s}$, BiOI/GH/FTO$_{-120s}$, BiOI/GH/FTO$_{-180s}$, respectively. The BiOI/FTO electrode was prepared at the same conditions with using a FTO as the working electrode.

4.2. Characterizations

The morphology and microstructure of the prepared sample were examined with the field emission gun scanning electron microscope (FE-SEM, Hitachi SU-8010) with an acceleration voltage of 100 kV. HRTEM images were obtained by JEM 2100 F field emission transmission electron microscope with an acceleration voltage of 200 kV. X-ray diffraction (XRD) patterns of BiOI/GH/FTO and BiOI/FTO electrodes were recorded at room temperature by using a Bruker D8 Advance X-ray diffractometer (Cu Kα, λ = 1.5406 Å, 40 kV, 40 mA). Raman spectra of as-pperpared samples were recorded on a microscopic confocal Raman spectrometer (HORIBA HR800, with an excitation of 514.5 nm laser light). The diffuse-reflectance spectrum (DRS) of BiOI/GH/FTO, GH/FTO and BiOI/FTO electrodes were recorded on an UV–vis spectrophotometer (Hitachi, U-3010) equipped with an integrated sphere, and $BaSO_4$ was used as the reference. The free radicals which generated in photoelectrocatalytic process were studied by trapping experiments. The concentration of phenol solution was determined by a high performance liquid chromatography (HPLC).

4.3. Photocatalysis, electrocatalysis and PEC degradation of 3D BiOI/GH/FTO electrodes

The photoelectrocatalytic and electrocatalytic degradation of the as-prepared 3D BiOI/GH/FTO electrodes were performed using a CHI660D (Shanghai, China) electrochemical workstation and a conventional three-electrode cell system connected with a Pt wire as the counter electrode and a saturated calomel electrode (SCE) as the reference electrode, BiOI/GH/FTO electrode and BiOI/FTO electrode as working electrodes. Phenol was used as the probe molecule with a concentration of 5 ppm. The visible light source (λ ≥ 420 nm) was provided by a xenon lamp (Perfectlight, filter, λ = 420 nm). The output light intensity was 500 mw/cm^2, and the received light intensity of working electrode was 225 mw/cm^2 with a distance between the light and working electrode was 18 cm.

***In static system*:** the photoelectrocatalytic degradation of phenol over different BiOI/GH/FTO electrodes were conducted under a certain voltage (E = 1.0 V). In order to study the influence of operating voltage on the synergistic effect of BiOI/GH/FTO electrode, the operating voltage varies from 0.8 V to 1.3 V. The volume of the reactor was 125 mL, and the volume of phenol solution was 100 mL with 0.1 M Na_2SO_4. The active area of BiOI/GH/FTO electrode was $2 \times 3\ cm^2$. And the photocatalytic activity, electrocatalytic activity and photoeletrocatalytic activity of BiOI/GH/FTO and BiOI/FTO electrodes were also evaluated by degrading phenol solution without Na_2SO_4 as the electrolyte.

***In dynamic system*:** the synergistic effect of photocatalytic degradation and electrocatalytic degradation of BiOI/GH/FTO$_{-60s}$ electrode was conducted under a certain voltage at E = 1.0 V. The effective area of BiOI/GH/FTO electrode was $2 \times 2.5\ cm^2$. The volume of homemade quartz reactor was 100 mL and the volume of phenol solution with a concentration of 5 ppm (without Na_2SO_4 electrolyte) was 80 mL. The flowing power was provided by a peristaltic pump with a speed of 4 r/min, and the flow rate of phenol solution is 1 mL/min.

4.4. Photoelectrochemical properties

The photoelectrochemical properties of electrode materials, such as transient photocurrents, were also measured on the electrochemical workstation (CHI-660D, China) with the three electrodes electrochemical system. The as-prepared BiOI/GH/FTO and BiOI/FTO electrodes served as the working electrodes, a platinum wire and SCE served as the counter and reference electrode, respectively. 0.1 M Na_2SO_4 solution was used as the electrolyte solution.

Acknowledgements

This work was partly supported by the National Natural Science Foundations of China (Grant No. 21577132), the Fundamental Research Funds for the Central Universities (Grant No. 2652015225) and the National Natural Science Foundations of China (21706091).

References

[1] W. Kujawski, A. Warszawski, W. Ratajczak, Desalination 163 (2004) 287–296.
[2] G. Wang, Q. Chang, X. Han, M. Zhang, J. Hazard. Mater. 248–249 (2013) 115.
[3] (a) H. Temmink, K. Grolle, Bioresour. Technol. 96 (2005) 1683;
(b) H.H. Fang, D.W. Liang, T. Zhang, Y. Liu, Water Res. 40 (2006) 427;
(c) A. Herzyk, P. Maloszewski, S. Qiu, M. Elsner, C. Griebler, Biodegradation 25 (2014) 325;
(d) F. Yamaga, K. Washio, M. Morikawa, Environ. Sci. Technol. 44 (2010) 6470.
[4] (a) T.-F. Lin, J.-K. Wu, Water Res. 35 (2001) 2049;
(b) J. Roosen, J. Spooren, K. Binnemans, J. Mater. Chem. A 2 (2014) 19415;
(c) V.M. Daskalaki, I. Fulgione, Z. Frontistis, L. Rizzo, D. Mantzavinos, Catal. Today 209 (2013) 74;
(d) Y. Tian, B. Chang, J. Lu, J. Fu, F. Xi, X. Dong, ACS. Appl. Mater. Interfaces 5 (2013) 7079;
(e) J. Xu, L. Wang, Y. Zhu, Langmuir 28 (2012) 8418.
[5] (a) M. Perez, F. Torrades, Appl. Catal. B Environ. 36 (2002) 63;
(b) A. Santos, P. Yustos, S. Gomis, Chem. Eng. Sci. 61 (2006) 2457;
(c) A. Alejandre, F. Medina, P. Salagre, Appl. Catal. B Environ. 18 (1998) 307.
[6] (a) A.M. Amat, A. Arques, F. Lopez, M.A. Miranda, Sol. Energy 79 (2005) 393;
(b) J.L. Boudenne, O. Cerclier, Appl. Catal. A Gen. 143 (1996) 185;
(c) A.V. Emelinea, X. Zhang, T. Murakami, A. Fujishimad, J. Hazard. Mater. 211–212 (2012) 154;
(d) H.Y. Jiang, X. Meng, H.X. Dai, J.G. Deng, Y.X. Liu, L. Zhang, Z.X. Zhao,

R.Z. Zhang, J. Hazard. Mater. 217–218 (2012) 92;
(e) H.Z. Ma, X.H. Zhang, Q.L. Ma, B. Wang, J. Hazard. Mater. 165 (2009) 475.
[7] (a) H. Huang, K. Xiao, Y. He, T. Zhang, F. Dong, X. Du, Y. Zhang, Appl. Catal. B Environ. 199 (2016) 75;
(b) Y. Wang, X. Wang, M. Antonietti, Angew. Chem. Int. Ed. 51 (2012) 68;
(c) H. Sun, G. Zhou, Y. Wang, A. Suvorova, S. Wang, ACS. Appl. Mater. Interfaces 6 (2014) 16745;
(d) F. Giordano, A. Abate, J.P. Correa Baena, M. Saliba, T. Matsui, S.H. Im, S.M. Zakeeruddin, M.K. Nazeeruddin, A. Hagfeldt, M. Graetzel, Nat. Commun. 7 (2016) 10379;
(e) Q. Xiang, J. Yu, M. Jaroniec, Chem. Soc. Rev. 41 (2012) 782.
[8] (a) M.R. Hoffmann, S.T. Martin, W.Y. Choi, D.W. Bahnemann, Chem. Rev. 95 (1995) 69;
(b) G. Chen, Sep. Purif. Technol. 38 (2004) 11.
[9] (a) H. Zheng, J.Z. Ou, M.S. Strano, R.B. Kaner, A. Mitchell, K. Kalantar-zadeh, Adv. Funct. Mater. 21 (2011) 2175;
(b) X. Zhao, J.H. Qu, H.J. Liu, C. Hu, Environ. Sci. Technol. 41 (2007) 6802;
(c) Y. Chen, X. Zhao, W. Guan, D. Cao, T. Guo, X. Zhang, Y. Wang, Chem. Eng. J. 324 (2017) 74;
(d) X. Zhao, L.B. Guo, C.Z. Hu, H.J. Liu, J.H. Qu, Appl. Catal. B Environ. 144 (2014) 478.
[10] (a) C. Janáky, K. Rajeshwar, Prog. Polym. Sci. 43 (2015) 96;
(b) C. Janáky, E. Kecsenovity, K. Rajeshwar, ChemElectroChem 3 (2016) 181.
[11] (a) J.C. Meyer, A.K. Geim, M.I. Katsnelson, K.S. Novoselov, T.J. Booth, S. Roth, Nature 446 (2007) 60;
(b) M.D. Stoller, S. Park, Y. Zhu, J. An, R.S. Ruoff, Nano Lett. 8 (2008) 3498.
[12] (a) A. Kongkanand, R. Martínez Domínguez, P.V. Kamat, Nano Lett. 7 (2007) 676;
(b) F. Meng, J. Li, S.K. Cushing, J. Bright, M. Zhi, J.D. Rowley, Z. Hong, A. Manivannan, A.D. Bristow, N. Wu, ACS Catal. 3 (2013) 746.
[13] (a) S. Yin, X. Men, H. Sun, P. She, W. Zhang, C. Wu, W. Qin, X. Chen, J. Mater. Chem. A 3 (2015) 12016;
(b) X. An, K. Li, J. Tang, ChemSusChem 7 (2014) 1086.
[14] (a) Z. Chen, W. Ren, L. Gao, B. Liu, S. Pei, H.M. Cheng, Nat. Mater. 10 (2011) 424;
(b) X.Y. Xiao, T.E. Beechem, M.T. Brumbach, T.N. Lambert, D.J. Davis, J.R. Michael, et al., ACS Nano 6 (2012) 3573;
(c) E. Kecsenovity, B. Endrődi, P.S. Tóth, Y. Zou, R.A.W. Dryfe, K. Rajeshwar, C. Janáky, J. Am. Chem. Soc. 139 (2017) 6682.
[15] (a) K. Chen, L. Chen, Y. Chen, H. Bai, L. Li, J. Mater. Chem. 22 (2012) 20968;
(b) S. Yang, Y. Huang, W. Zhu, B. Deng, H. Wang, Z. Zhang, P. Bao, G. Wang, Int. J. Hydrogen Energy 39 (2014) 15063.
[16] T.W. Kim, K.-S. Choi, Science 343 (2014) 990.
[17] K.-H. Ye, Z. Chai, J. Gu, X. Yu, C. Zhao, Y. Zhang, W. Mai, Nano Energy 18 (2015) 222.
[18] E. Kecsenovity, B. Endrődi, P.S. Tóth, Y. Zou, R.A.W. Dryfe, K. Rajeshwar, C. Janáky, J. Am. Chem. Soc. 139 (2017) 6682.
[19] D. Liu, J. Wang, X. Bai, R. Zong, Y. Zhu, Adv. Mater. 28 (2016) 7284.
[20] (a) R. Hao, X. Xiao, X. Zuo, J. Nan, W. Zhang, J. Hazard. Mater. 209–210 (2012) 137;
(b) L.-S. Zhang, K.-H. Wong, H.-Y. Yip, C. Hu, J.C. Yu, C.-Y. Chan, P.-K. Wong, Environ. Sci. Technol. 44 (2010) 1392.
[21] T. Tan, D. Beydoun, R. Amal, J. Photochem. Photobiol. C 159 (2003) 273.
[22] Y. Li, J. Wang, H. Yao, L. Dang, Z. Li, J. Mol. Catal. A Chem. 334 (2011) 116.
[23] K. Sheng, Y. Sun, C. Li, W. Yuan, G. Shi, Sci. Rep. 2 (2012) 247.